DOI: 10.2478/v10077-011-0016-6

Matthieu Dhondt[1,2]**, Isabelle Aubert**[1]**, Nicolas Saintier**[2]**, Jean-Marc Olive**[3]

[1]*Université de Bordeaux, I2M-Dumas, UMR 5295, 351 cours de la Libération 33405 TALENCE CEDEX FRANCE*
[2]*Art et Métier ParisTech (Centre de Bordeaux-Talence), I2M-Dumas, UMR 5295, Esplanade des Arts et Métiers 33405 Talence Cedex FRANCE*
[3]*CNRS, I2M-Dumas, UMR 5295, 351 cours de la Libération 33405 TALENCE CEDEX France*
m.dhondt@i2m.u-bordeaux1.fr

INTERGRANULAR STRESS CORROSION CRACKING OF FRICTION STIR WELDED NUGGET ON A 2050-T8 ALUMINUM ALLOY

ABSTRACT

Intergranular corrosion sensitivity is studied for the friction stir weld nugget of aluminum alloy 2050-T8. The weld nugget consists of fine equiaxed grains having average sizes from 4 to 20 µm, the grain size increases with decreasing of the distance from the weld surface. The weld nugget contains a particular microstructure called “onion rings” due to crystallographic orientations. The effect of the “onion rings” on stress corrosion cracks initiation is studied for stress corrosion cracking tests at a strain rate of 2.10^{-6} s^{-1}. EBSD cartographies allow showing that the initiation site of the biggest cracks is located at boundaries between the texture bands. Corrosion and stress corrosion tests in 1.0 M NaCl are performed in order to show stress effect on intergranular corrosion. Pitting corrosion is observed during corrosion tests, whereas intergranular cracks appear during stress corrosion tests. The medium crack length is 20 µm and 168 cracks per mm^2 can be located. In these severe laboratory conditions, the order of magnitude of long crack growth rate is 5.10^{-8} $m.s^{-1}$.

Keywords: *Aluminum alloy, intergranular stress corrosion cracking, Friction Stir Welding*

INTRODUCTION

To reduce weight of some structures components in the aircraft industry, two solutions are explored. The first one is based on substitution of 7xxx aluminum alloys by aluminum-copper-lithium alloys 2050 which have a lower density and similar proprieties (corrosion, fatigue, tenacity …). The second one is the substitution of riveting by Friction Stir Welding (FSW). This welding method, without fusion, was developed by the Welding Institute (TWI) in 1991 and could favorably replace riveting.

As every welding process, FSW induces microstructural changes due to the plastic deformation and frictional heat. On the weld joint, three distinct zones with specific

microstructures [1-5] exist namely: heat affected zone (HAZ), thermo-mechanically affected (TMAZ) zone and weld nugget (WN).
Thermo-mechanical history on the weld joint induces gradients in mechanical and corrosion behavior. Microhardness variations exist in those different zones [1-3, 5-7]. The microhardness profiles found in the literature depend on the alloy chemical composition, on the thermal treatment before and after welding and on the welding conditions. The corrosion behavior is also different in each zone; there is a significant variation of open circuit potential all across the weld [1-2, 6]. The nugget zone and the TMAZ, including a part of the HAZ, are the most electronegative zones compare to the base material.
This study is exclusively focused on the weld nugget of the alloy. The nugget region consists of fine equiaxed grains due to dynamic recrystallisation whereas the neighboring zones consist of elongated grains [1-8]. The weld nugget contains one of the most characteristic features of friction stir welds – the "onion rings" structure [9-10]. These concentric elliptical surfaces have a periodicity along the welding direction corresponding to the advance per revolution of the tool and can be correlated to a texture variation [10].

MATERIAL OF THE STUDY

The material of this study is the nugget of a 2050 aluminum alloy welded to a T3 metallurgical state (solutionising, quenching and stretching) and submitted to a post-welding heat treatment which consists of a T8 over-aged heat treatment. A previous study [1] showed the beneficial effect of this post-welding treatment on the corrosion behavior of the material. The grain size goes from 4 to 20 μm and increases with decreasing of the distance from the weld surface.
This project is focused on the corrosion behavior of the material at local scale. First industrial tests show that this material may show some sensitivity to intergranular corrosion in specific conditions. Intergranular corrosion can depend on several parameters as precipitation [11], crystallographic orientations [12-13] or mechanical stress application [14]. In this document, corrosion tests are presented in order to underline some parameters effect (external stress, internal stress and microstructure).

SAMPLE AND EXPERIMENTAL PROCEDURE

Tensile test specimens (fig. 1) are machined in the longitudinal direction of the weld nugget. Before each test, the samples are mechanically polished down to 1 μm with a diamond paste. The traction tests are made at imposed displacement rate. To limit the phenomenon of low stress corrosion, the corrosive solution is introduced for a stress higher than the yield stress. Above the yield stress, the test is continuing at a strain rate of 2.10^{-6} s^{-1}.
Internal stress effect is valued on a sample pre-strained in air (after a plastic strain of 12%) submitted to the corrosive solution. At a relaxed state, internal stresses exist on a pre-strained sample due to strain incompatibilities at microscopic scale. For the tests with pre-straining, the samples are polished again before immersion in order to eliminate roughness due to plastic strain. For all the tests, the corrosive solution is a 1.0 M NaCl aerated solution at room temperature. The total exposition time to the NaCl solution is fixed and equal to 1h30 for the tests.

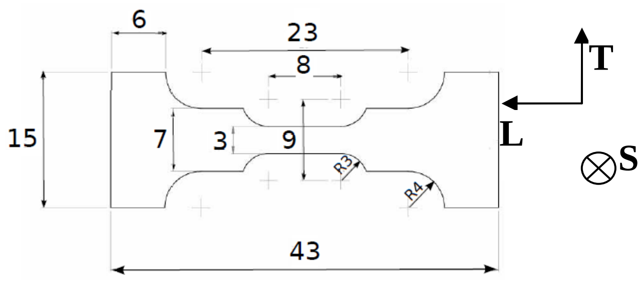

Fig. 1. Traction sample dimension

EXTERNAL/INTERNAL STRESS EFFECT

SEM images shown in fig. 2 reveal that the weld nugget is sensitive to pitting corrosion in a 1.0 M NaCl aerated solution at room temperature when it is not submitted to a mechanical loading (fig. 2a). A stress application induces a change in corrosion mode from pitting to intergranular stress corrosion cracking (fig. 2b and 2c). The shape of those cracks depends on whether the applied stress is external or internal. In the first case (fig. 2b), a typical IG-SCC initiation and propagation normal to the loading axis is observed. In the second case (fig. 2c), the stress level after relaxation is lower than during the slow strain rate test, intergranular cracks have no preferential directions.

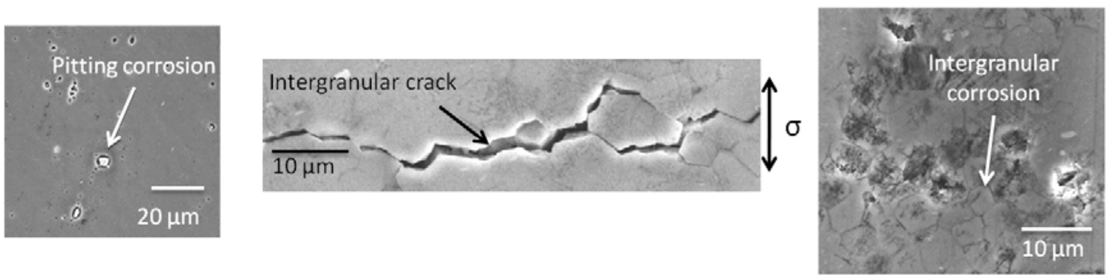

(a) (b) (c)

Fig. 2. SEM images (a) After the corrosion test (b) After the stress corrosion test (c) After the corrosion test on the pre-strained sample

The slow strain rate test reveals initiation of several cracks distributed in lengths and locations. A statistical analysis was made on the area shown in fig. 3 and the crack density is estimated to 168 cracks per mm². The crack lengths repartition is shown in fig. 4 and the medium crack length is 20 µm. On the fig. 4, the black curve represents the theoretical log normal distribution that is defined by the probability density function Eq. (1).

$$f(x) = \frac{1}{E_{\ln(x)} x \sqrt{2\pi}} e^{-(1/2)\left(\left(\ln(x) - m_{\ln(x)}\right)/E_{\ln(x)}\right)^2} \tag{1}$$

Where $m_{\ln(x)}$ and $E_{\ln(x)}$ are the mean and standard deviation of the variable ln(x) respectively. In this case, $m_{\ln(x)}$=2,39 and $E_{\ln(x)}$=0,99. The crack length (l) distribution is well approximated by the log normal law. That is to say ln(l) follow a normal distribution. The magnitude of long crack growth rate can be evaluated by considering that long cracks initiate when the NaCl solution is introduced. The order of this value is 5.10^{-8} m.s^{-1}.

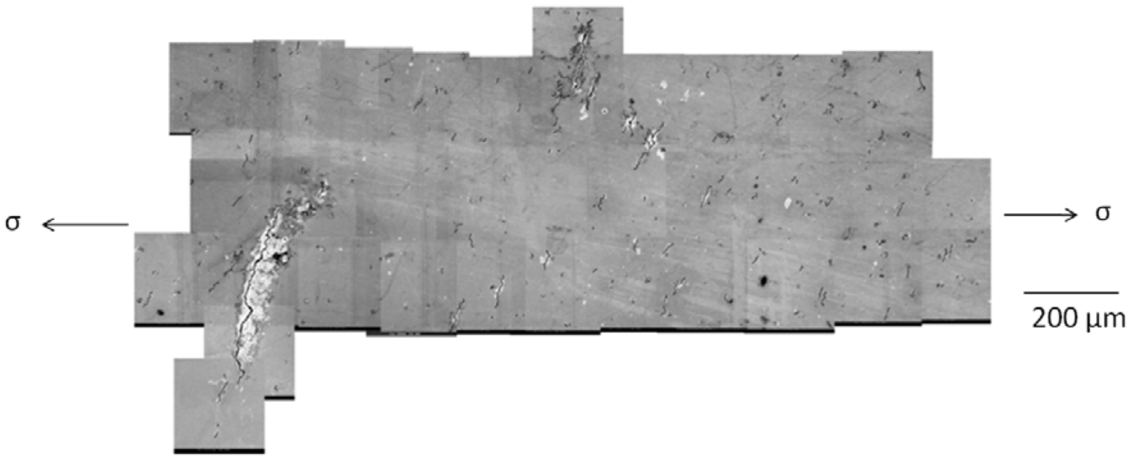

Fig. 3. IG-SCC on the sample submitted to slow strain rate test in 1.0 M NaCl aerated solution at room temperature (SEM images)

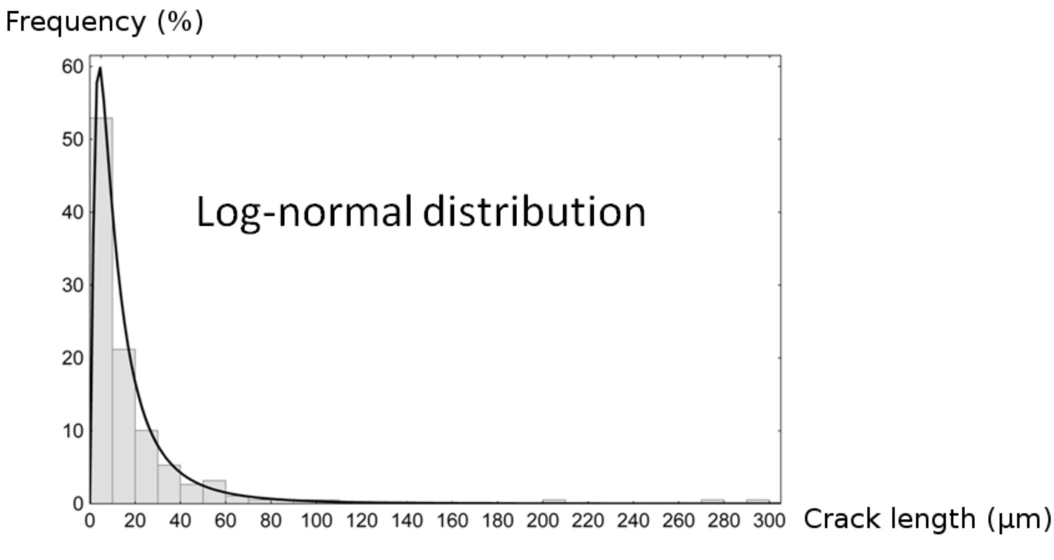

Fig. 4. Crack length repartition in the sample

MICROSTRUCTURE EFFECT

The "onion rings" of the material are revealed by an electrolytic attack and are correlated to a texture variation thanks to EBSD cartographies (fig. 5). This texture variation induces plastic strain heterogeneities into the sample. A traction test is made on a sample taken on the (T,L) direction to underline this phenomenon. The stress-strain curve is shown in fig. 6. An optic image after the test is shown in fig. 7a and illustrated in fig. 7b. This figure reveals shearing bands and deformation bands (type A and type B) initiation. Deformation bands can be associated to the "onion rings" shown in fig. 5. The boundary between type A and type B deformation bands is analyzed under AFM (fig. 8). This AFM topography reveals a specific roughness along the boundary between the two deformation bands. This is probably connected with strong heterogeneities of strain/stress fields at the boundary between zones of different crystallographic textures. These bands boundaries seem to act as preferential site for intergranular stress corrosion cracks initiation. This effect is checked for the sample which is submitted to the stress corrosion cracking test. A polishing down to ¼ µm after the test allow obtaining a correct suitable surface to make EBSD cartographies next to the intergranular stress corrosion cracks. An optic image and EBSD cartographies next to the cracks are shown in fig. 9. EBSD cartographies reveal microstructure bands and show that long cracks initiate at bands boundaries.

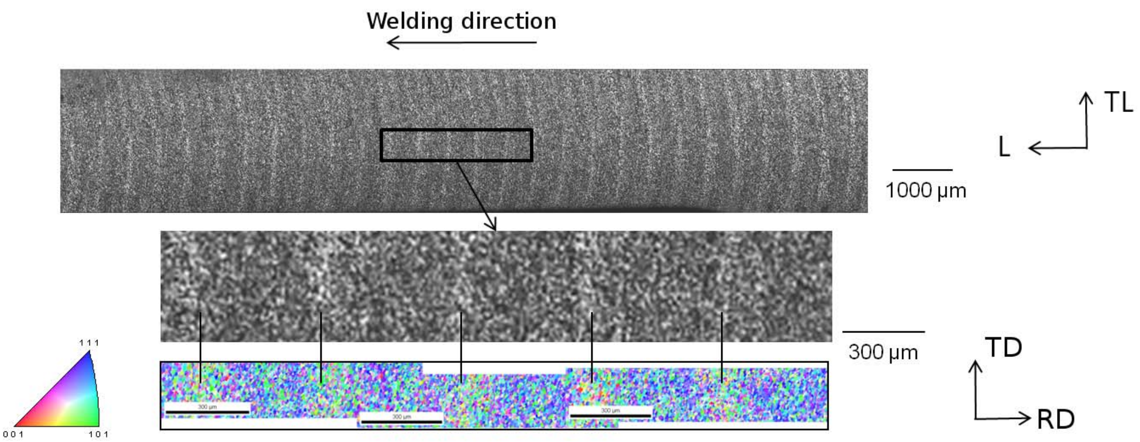

Fig. 5. Optic image of the weld nugget microstructure (L,T plan) after electrolytic attack and EBSD cartography

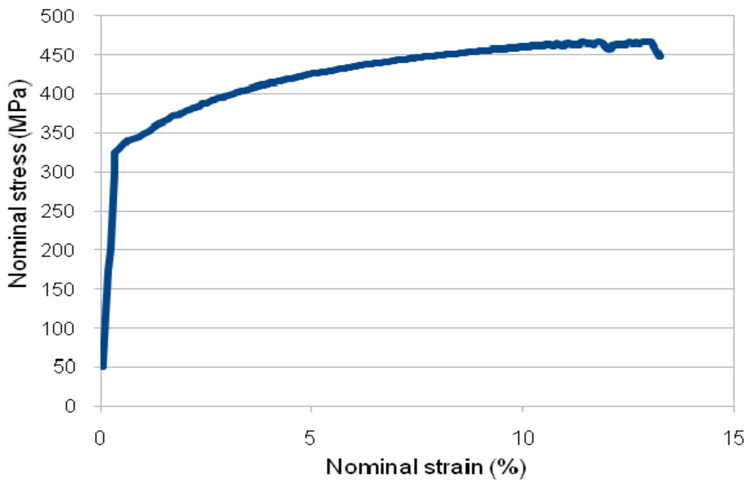

Fig. 6. Stress-strain curve in air

Fig. 7. (a) Optic image of the sample after the traction test (b) Schematic representation of the sample surface

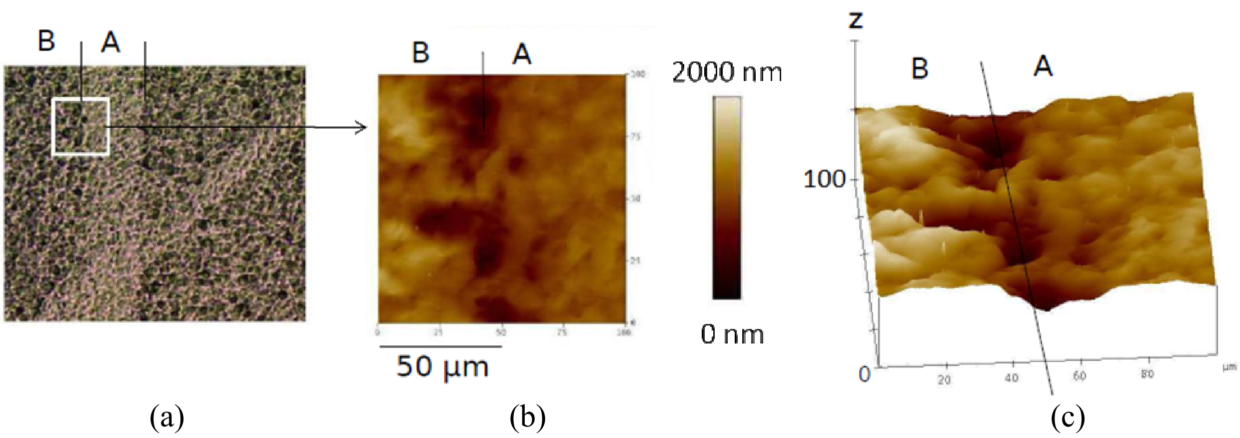

Fig. 8. (a) Optic image of a zone including a type A deformation band and type B one (b) 2D AFM topography at deformation bands boundary (c) Corresponding 3D AFM topography

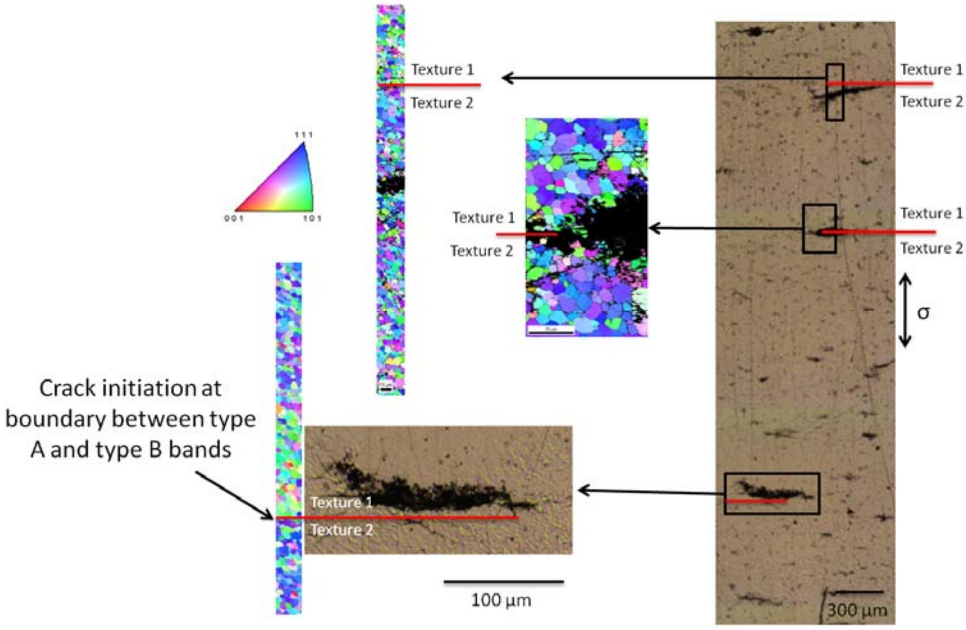

Fig. 9. Optic image of sample which was submitted to stress corrosion test and EBSD cartographies next to the crack

SUMMARY

Laboratory accelerated corrosion tests reveal that the nugget of FSW joint is sensitive to pitting corrosion in 1.0 M NaCl aerated solution at room temperature when no stress is applied. Stress corrosion cracking tests (SSRT) show a change in corrosion mode from pitting to intergranular stress corrosion cracks. Immersion tests on pre-strained sample also reveal initiation of intergranular stress corrosion cracks but cracks have a different shape due to the stress field characteristics.

“Onion rings” lead to the existence of preferential sites for intergranular stress corrosion cracks initiation when an external stress is applied. Other parameters effects on intergranular corrosion of the material have to be investigated. Grain size heterogeneities, grain boundaries misorientation and local stress have to be taken into account. Finite Element Modeling is being developed in order to simulate intergranular stress corrosion cracking initiation and propagation.

ACKNOWLEDGMENTS

This work was financially supported by the ANR MatetPro program ANR-08-MAPR-0020-05 (Coralis project, Corrosion of Aluminium Lithium Structures). The authors would like to acknowledge Jérémie BEGA (ENSAM) for his help.

REFERENCES

1. Proton V., Alexis J., Andrieu E., Blanc C., Delfosse J., Lacroix L., Odemer G. : Influence of Post-Welding Heat Treatment on the Corrosion Behavior of a 2050-T3 Aluminum-Copper-Lithium Alloy Friction Stir Welding Joint. Journal of The Electrochemical Society 158 (5) (2011) C139-C147.

2. Fonda R.W., Pao P.S., Jones H.N., Feng C.R., Connolly B.J., Davenport A.J.: Microstructure, mechanical properties, and corrosion of friction stir welded Al 5456. Materials Science and Engineering A 519 Issues 1-2 (2009) 1-8.

3. Genevois C.: Genèse des microstructures lors du soudage par friction malaxage d'alliages d'aluminium de la série 2000 et 5000 et comportement mécanique resultant. PhD thesis, Institut National Polytechnique de Grenoble (2004).

4. Zhou C., Yang X., Luan G.: Effect of root flaws on the fatigue property of friction stir welds in 2024-T3 aluminum alloys. Materials Science and Engineering A 418 (2006) 155-160.

5. Jariyaboon M., Davenport A.J., Ambat R., Connolly B.J., Williams S.W., Price D.A.: The effect of welding parameters on the corrosion behaviour of friction stir welded AA2024–T351. Corrosion Science 49 (2007) 877-909.

6. Cavaliere P., Cabibbo M., Panella F., Squillace A.: 2198 Al–Li plates joined by Friction Stir Welding: Mechanical and microstructural behavior. Materials and Design 30 (2009) 3622–3631

7. Bousquet E., Puiggali M., Poulon-Quintin A., Devos O., Touzet M.: Correlation between microstructure, microhardness and corrosion sensitivity of AA 2024-T3 FSW weld-joints. In Eurocorr 2010 The European Corrosion Congress.

8. Jata K.V., Semiatin S.L.: Continuous dynamic recrystallization during friction stir welding of high strength aluminum alloys. Scripta materialia 43 (2000) 743-749.

9. Sutton M.A., Yang B., Reynolds A.P., Taylor R.: Microstructural studies of friction stir welds in 2024-T3 aluminum. Materials Science and Engineering A 323 (2002) 160-166.

10. Fonda R.W., Bingert J.F.: Texture variations in an aluminum friction stir weld. Scripta Materialia 57 (2007) 1052-1055.

11. Li J.F., Li C.X., Peng Z.W., Chen W.J., Zheng Z.Q.: Corrosion mechanism associated with T1 and T2 precipitates of Al–Cu–Li alloys in NaCl solution. Journal of Alloys and Compounds 460 (2008) 688–693.

12. Miyamoto H., Ikeuchi K., Mimaki T.: The role of grain boundary plane orientation on intergranular corrosion of symmetric and asymmetric [1 1 0] tilt grain boundaries in directionally solidified pure copper. Scripta Materialia 50 (2004) 1417–1421.

13. Kim S.H., Erb U., Aust K.T., Palumbo G.: Grain boundary character distribution and intergranular corrosion behavior in high purity aluminum. Scripta mater. 44 (2001) 835–839.

14. Liu X., Frankel G.S., Zoofan B., Rokhlin S.I.: Effect of applied tensile stress on intergranular corrosion of AA2024-T3. Corrosion Science 46 (2004) 405–425.